Chem

CellPress

Article

Expanding the architectural horizon of nucleic-acid-polymer biohybrids by site-controlled incorporation of ATRP initiators in DNA and RNA

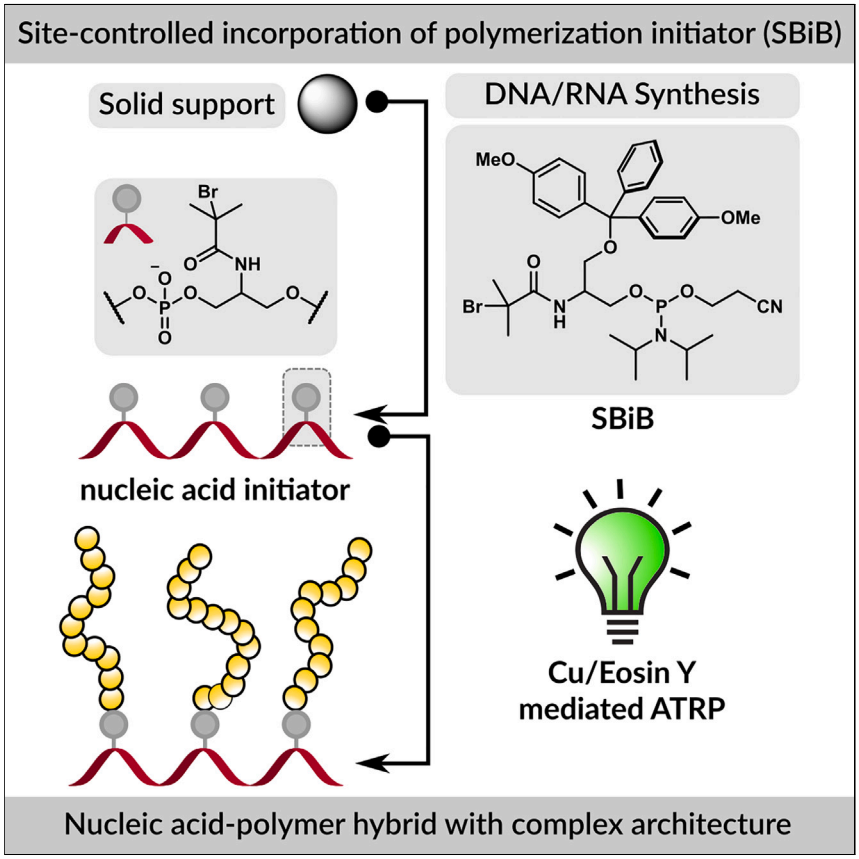

Matyjaszewski, Das, and co-workers have synthesized and incorporated SBiB, a serinol-based ATRP-initiator-functionalized phosphoramidite, into nucleic acids during solid-phase synthesis in a site-controlled manner. They demonstrate that polymers can be grown from one or multiple SBiB residues integrated into nucleic acids with a narrow molecular-weight distribution. This method expands the architectural scope of nucleic-acid-polymer hybrids beyond simple diblock copolymers.

Jaepil Jeong, Grzegorz Szczepaniak, Subha R. Das, Krzysztof Matyjaszewski

srdas@andrew.cmu.edu (S.R.D.)
km3b@andrew.cmu.edu (K.M.)

Highlights

Serinolic ATRP-initiator-functionalized phosphoramidite was synthesized

Multiple SBiBs were incorporated in nucleic acids during solid-phase synthesis

Photo-ATRP from SBiB in nucleic acid initiators yields well-defined hybrids

Jeong et al., Chem 9, 3319–3334
November 9, 2023
https://doi.org/10.1016/j.chempr.2023.07.013

Chem

CellPress

Article

Expanding the architectural horizon of nucleic-acid-polymer biohybrids by site-controlled incorporation of ATRP initiators in DNA and RNA

Jaepil Jeong,[1,2] Grzegorz Szczepaniak,[1,3] Subha R. Das,[1,2,*] and Krzysztof Matyjaszewski[1,4,*]

SUMMARY

Modifying biomacromolecules with synthetic polymers has been a powerful approach to developing multifunctional hybrid biomaterials for nanoscience and biomedical applications. With oligonucleotides, limited coupling and conjugation strategies were replaced with approaches allowing for the initiation of polymer chains directly from a terminus of synthetic DNA sequences. Although these strategies have provided access to diblock (DNA-polymer) bioconjugates, oligonucleotide biohybrids with more complex architectures have remained challenging. In this work, we vastly expand the possibility of creating diverse oligonucleotide-polymer biohybrids by developing serinol-based α-bromoisobutyryl (SBiB) phosphoramidite. This universal reagent allows for multiple site-specific incorporations of an atom-transfer radical polymerization (ATRP) initiator within a synthetic DNA or RNA sequence. Combining this methodology with the recently developed green-light-induced ATRP with dual catalysis has enabled the precise fabrication of well-defined, complex hybrid nucleic acid polymers.

INTRODUCTION

Combining biomacromolecules with synthetic polymers has created new classes of biomaterials that exhibit the properties of both natural and synthetic components.[1–4] These molecular chimeras often exhibit synergetic and enhanced properties, such as hyperstability.

Engineering of nucleic-acid-polymer hybrids (NAPHs) architecture beyond simple diblock copolymers (e.g., multiblock copolymers, miktoarm stars, and bottlebrush polymers) has proved to be a fascinating route for tailoring their self-assembly,[5–12] mechanical and optical properties,[13–18] pharmacokinetics,[19–23] and pharmacodynamics.[24–27] To be specific, the micro-miscibility of DNA- poly(*N*-isopropylacrylamide) (DNA-pNIPAM) conjugates can be controlled by the incorporation of the pNIPAM chain into different positions in DNA. For example, the use of rod-like pNIPAM-DNA-pNIPAM triblock copolymers and π-shaped branched conjugates allows for the modulation of self-assembly, enabling the formation of various bicontinuous phases beyond lamellar structures.[6] Additionally, the incorporation of PEG (polyethylene glycol) chains or their analogs at both the 5′ and 3′ termini of DNA[24] and RNA[28] or within the middle region[20] has improved the degradation resistance of the nucleic acid to nucleases (exo- or endonucleases) and allowed self-delivery to cells, resulting in enhanced therapeutic efficacy.

Until recently, architecture control has been mainly done through the incorporation of pre-synthesized polymers into the desired site of the oligonucleotide sequence

THE BIGGER PICTURE

Polymer biohybrids are modern synthetic molecular chimeras. These hybrids exhibit enhanced sequence specificity of nucleic acids and improved functionality of synthetic polymers. However, their formation is limited to grafting polymer chains to the terminus of nucleic acid strands. Herein, we present a new reagent, serinol-based α-bromoisobutyryl (SBiB) phosphoramidite, that allows for multiple incorporations of a polymer initiator moiety anywhere in an oligonucleotide, including both DNA and RNA sequences. Combining the SBiB-based phosphoramidite chemistry with the recently developed photoredox/copper-catalyzed atom-transfer radical polymerization (ATRP) technique greatly expands the scope of DNA- and RNA-polymer hybrids that can be created. By leveraging this new approach, researchers can now obtain a much wider variety of polymer biohybrids that could have potential applications in biomedicine, materials science, and beyond.

via coupling reactions such as Cu(I)-catalyzed azide-alkyne cycloaddition (CuAAC), strain-promoted azide-alkyne click chemistry (SPAAC), amide bond formation, base paring, or enzymatic incorporation. These methods, referred to as the "grafting-to" approach, allow the synthesis of block copolymers or simply branched hybrids.[6,18,29–31] However, access to NAPHs with more complex architectures is limited by steric hindrance and solubility differences between the nucleic acids and synthetic polymers.[32–36] As a consequence, control over the grafting density or the number of polymer chains remains challenging despite the specificity of the coupling chemistry. Hence, such polymer tethers are often limited to low-molecular-weight polymers or oligomers.[26,37–40] Moreover, the grafting-to approach requires the separation of the unreacted polymers, which further impedes the expansion of the field.

A promising alternative is the "grafting-from" method, where polymerization is initiated from the host biomolecule. This approach expands the range of complexity by significantly reducing the steric challenge.[41–45] Atom-transfer radical polymerization (ATRP) and reversible addition-fragmentation transfer (RAFT) polymerization are the most widely used polymerization techniques for growing well-defined polymers from, or in the presence of, biomolecules,[46–48] exosomes,[49,50] and cells[43,51,52] because of their controlled radical polymerization behavior.[53] In ATRP, the polymer chain is grown from an alkyl halide initiator (R-X, where X = Cl or Br) through the reversible activation and deactivation processes typically mediated by copper catalysts. In contrast, RAFT polymerization is mediated and controlled by a chain-transfer agent (CTA). Nevertheless, the precise positioning of multiple initiators (for ATRP) or CTAs (for RAFT) within the host nucleic acids and the purification of the final product have been challenging. As a consequence, to date, most reports by us and other groups have been restricted to the nucleic-acid-block copolymers.[1] Therefore, a technique for the successful synthesis of precision NAPHs with the desired architecture needs to address the following challenges: (1) direct and site-controlled incorporation(s) of polymer moieties, (2) facile purification of the desired product, and (3) the grafting of well-defined polymers with desired dispersity and length.

To address these challenges and expand the architectural horizon of nucleic-acid-polymer biohybrids, we were inspired by phosphoramidite chemistry, a widely used method for oligonucleotide synthesis.[54,55] Through the sequential coupling of phosphoramidite building blocks to the oligonucleotide chain on the solid support, phosphoramidite chemistry has been the gold standard for synthesizing sequence-defined DNA and RNA with functional moieties in the desired location.[56,57] In this study, we developed a serinol-based α-bromoisobutyryl (**SBiB**) phosphoramidite that can be used for precisely incorporating single, or even multiple, ATRP initiators into an oligonucleotide strand at any location(s). The α-bromoisobutyryl ATRP initiator, instead of CTA for RAFT, was chosen for functionalization to the phosphoramidite analog because of the potential hydrolysis of typical dithioester-based CTA during the cleavage of the DNA (or RNA) from solid support. We demonstrate using automated solid-phase DNA/RNA synthesis with one or multiple **SBiB** phosphoramidites incorporated into the sequence at single-nucleotide precision. This methodology provides a facile, robust, and automated strategy for the preparation of DNA- or even RNA-**SBiB** initiators, which are the requisite precursors for NAPHs. It should be noted that engineering the architecture of RNA-polymer hybrids has been less explored than engineering DNA-polymer hybrids, and only a few examples of grafting from RNA[47] or RNA-triblock copolymer[28] have been reported. We also demonstrate that **SBiB**-based phosphoramidite chemistry can

[1]Department of Chemistry, Carnegie Mellon University, Pittsburgh, PA, USA

[2]Center for Nucleic Acids Science & Technology, Carnegie Mellon University, Pittsburgh, PA, USA

[3]Faculty of Chemistry, University of Warsaw, Pasteura 1, Warsaw, Poland

[4]Lead contact

*Correspondence: srdas@andrew.cmu.edu (S.R.D.), km3b@andrew.cmu.edu (K.M.)

https://doi.org/10.1016/j.chempr.2023.07.013

be combined with green-light-induced ATRP via dual catalysis for grafting well-defined polymer chains, vastly expanding access to NAPHs with complex architectures.

RESULTS AND DISCUSSION

Synthesis and incorporation of SBiB in DNA

To develop a phosphoramidite reagent with an ATRP initiator that could be used in subsequent and multiple coupling cycles during solid-phase oligonucleotide synthesis, we selected serinol as the starting material because it has a three-carbon chain along with all the required functional groups. This includes the hydroxyl group required for installing the 2-cyanoethyl *N*,*N*-diisopropyl phosphoramidite for coupling, a primary amine needed for attaching the α-bromoisobutyrate ATRP initiator, and a second hydroxyl group, protected with a dimethoxytrityl (DMT) group, needed for extending the sequence.

First, α-bromoisobutyryl bromide (BiBB) was attached to the primary amine in serinol (Figure 1A), resulting in the intermediate compound **1** (Figure S1). Then, one of the hydroxyl groups was protected with the DMT group to yield **2** (Figure S2). Finally, the reaction with 2-cyanoethyl *N*,*N*-diisopropylchlorophosphoramidite yielded the desired **SBiB** phosphoramidite as a pale-yellow viscous oil. The structure of the final product was confirmed by ^{1}H NMR (Figure S3) and ^{31}P NMR (Figure S4).

It is noteworthy that the **SBiB** phosphoramidite could be used along with standard DNA and RNA phosphoramidites and reagents without modification of the coupling conditions, demonstrating its universality (Table S1). During solid-phase DNA synthesis in an oligonucleotide synthesizer, the **SBiB** phosphoramidite was coupled to the 5′-OH on the growing DNA chain (Figure 1B). In the next step, the DMT group in the incorporated **SBiB** was removed with trichloroacetic acid. Then, the deprotected hydroxyl group was used for coupling the next phosphoramidite, which could be either a standard DNA and RNA phosphoramidite or another **SBiB** phosphoramidite. Thus, this automated, site-controlled, and direct coupling of **SBiB** allowed the incorporation of a polymerization initiator at any desired location within an oligonucleotide sequence, as well as made multiple incorporations possible for the first time. After the synthesis, the oligonucleotide-**SBiB** was cleaved from the solid support, deprotected, desalted, and purified. A significant additional benefit of the **SBiB** phosphoramidite, even for terminal attachment, is the facile removal of truncated sequences during the desalting step. The final product with the DMT group can be purified by the standard reverse-phase DMT-on desalting process, during which truncated sequences lacking the terminal DMT (having an acetyl group instead of DMT) can be removed during the washing step (Table S2).[58,59]

Polymerization from the middle of an oligonucleotide sequence

With the ability to incorporate the **SBiB** within sequences, we next explored the possibility of using the DNA-**SBiB** as the model macroinitiator for the recently developed green-light-induced ATRP via dual catalysis. This technique allows controlled aqueous polymerization at a low reaction volume of 250 μL without any deoxygenation process (Figure S6).[60] First, a model oligothymidine that included one **SBiB** initiator in the middle of a T8 sequence was prepared (T4-**SBiB**-T4). Oligo(ethylene oxide) methyl ether methacrylate (average M_n = 500, $OEOMA_{500}$) was used as a model monomer, eosin Y (EYH_2) was used as the photoredox catalyst, and $CuBr_2$/TPMA (TPMA = tris(2-pyridylmethyl) amine) was used as the deactivator. The polymerizations were carried out in phosphate-buffered saline (PBS) solution under the irradiation of green light-emitting diodes (LEDs) (λ = 520 nm, 3.7 mW cm^{-2}) (Table 1).

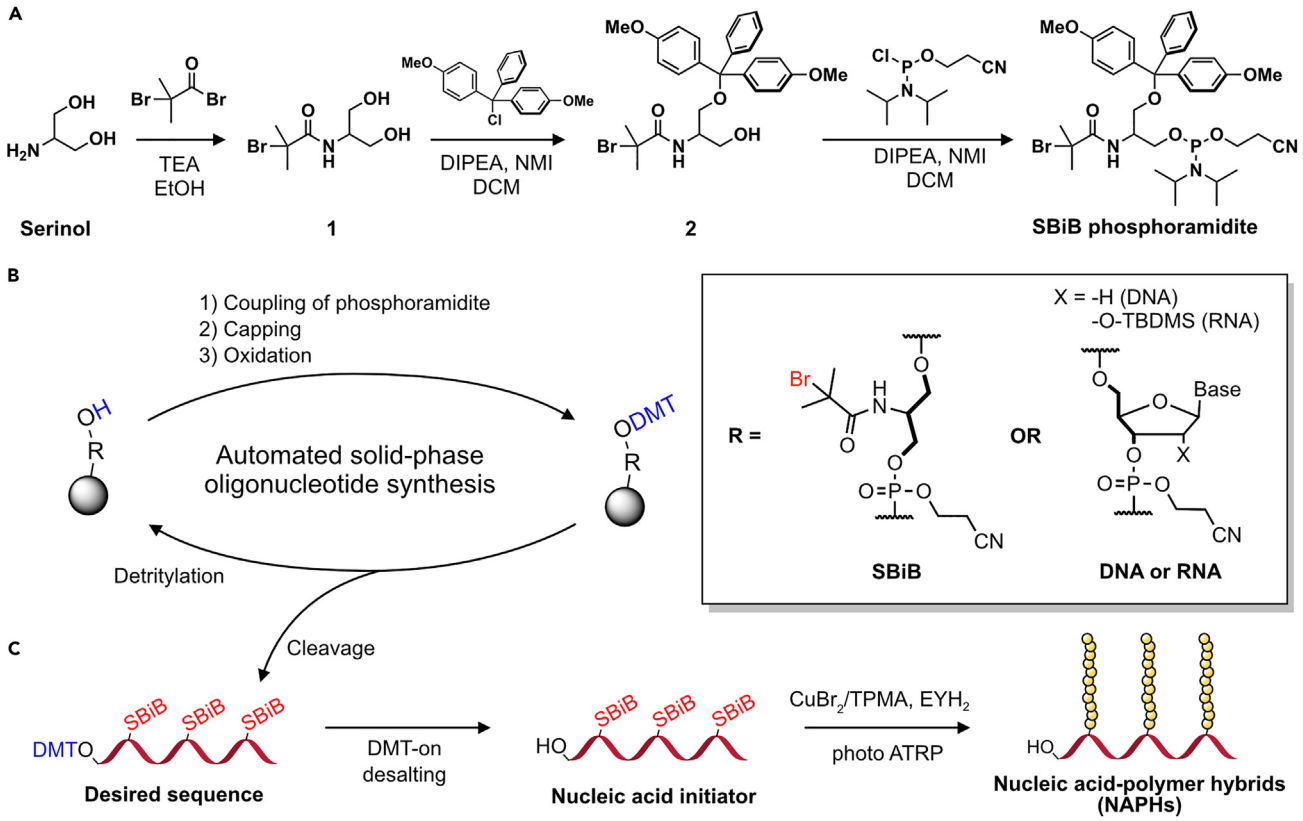

Figure 1. Synthesis and solid-phase incorporation of SBiB and polymerization from oligonucleotide initiator

(A) Scheme for the synthesis of the **SBiB** phosphoramidite.

Abbreviations are as follows: Me, methyl group; TEA, triethylamine; EtOH, ethanol; DIPEA, *N*,*N*-diisopropylethylamine; NMI, *N*-methylimidazole; DCM, dichloromethane.

(B) Scheme of solid-phase incorporation of **SBiB** and standard DNA or RNA phosphoramidites using an oligonucleotide synthesizer. The inset shows the structure of the incorporated residue. Identical coupling conditions for standard DNA and RNA phosphoramidites were applied for **SBiB** coupling.

Abbreviations are as follows: DMT, dimethoxytrityl group; TBDMS, *tert*-butyldimethylsilyl group.

(C) After the solid-phase synthesis, oligonucleotide cleavage and deprotection of phosphate- and base-protecting groups were performed. The DMT group on the desired final product's terminus was utilized as a hydrophobic tag for reverse-phase purification of the oligonucleotide initiator during the standard DMT-on desalting process. Fully deprotected and desalted oligonucleotide initiator was mixed with $CuBr_2$, TPMA, and EYH_2 for polymer growth via ATRP under green-light irradiation in PBS.

We selected PBS as the reaction medium to ensure benign conditions and convert EYH_2 to its photoactive form (EY). The sequences of all the oligonucleotides used in this study are shown in Table S3.

We started our study by comparing three different initiators—2-hydroxyethyl α-bromoisobutyrate (HEBiB), free **SBiB** phosphoramidite, and the T4-**SBiB**-T4—in green-light-induced ATRP by using molar ratios of $[OEOMA_{500}]/[initiator]/[EYH_2]/[CuBr_2]/[TPMA] = 600/1/0.0/0.6/1.8$ (Table 1, entries 1–3). All three initiators yielded well-defined polymers with narrow molecular-weight distributions ($Đ < 1.35$). Notably, when the T4-**SBiB**-T4 initiator was used (Table 1, entry 3), the monomer conversion and the dispersity were higher than with HEBiB (Table 1, entry 1) or free **SBiB** (Table 1, entry 2) as the initiator. This could be attributed to the poor halidophilicity of $[Cu^{II}/L]^{2+}$ complexes in aqueous media.[61,62] The loss of halogen (X) in the $[X–Cu^{II}/L]^{+}$ deactivator could cause electrostatic binding of $[Cu^{II}/L]^{2+}$ to the DNA backbone. To test our hypothesis, we conducted polymerization from the T4-**SBiB**-T4 macroinitiator with additional NaCl (final concentration of 340 mM) to suppress dissociation

Table 1. Polymerization conditions for grafting from DNA macroinitiator and dispersity control

Entry	Initiator	[$CuBr_2$]/[TPMA]	[Cu^{2+}]	Conversion[a]	$M_{n,th}$	$M_{n,abs}$[b]	$M_{n,GPC}$[c]	$Đ$[c]
1	HEBiB	0.6 /1.8	0.3 mM	70%	210,211	230,000	149,000	1.20
2	Free **SBiB**[d]	0.6/1.8	0.3 mM	53%	159,723	182,000	123,000	1.17
3	T4-**SBiB**-T4	0.6/1.8	0.3 mM	80%	242,970	416,000	243,000	1.35
4	T4-**SBiB**-T4[e]	0.6/1.8	0.3 mM	67%	203,970	199,000	132,100	1.27
5	T4-**SBiB**-T4	1.0/3.0	0.5 mM	71%	215,970	317,000	194,200	1.32
6	T4-**SBiB**-T4	1.4/4.2	0.7 mM	67%	203,970	260,000	165,100	1.29
7	T4-**SBiB**-T4	1.8/5.4	0.9 mM	57%	173,970	194,000	129,700	1.23
8	T4-**SBiB**-T4	2.4/7.2	1.2 mM	55%	167,970	122,000	88,500	1.20

Reaction conditions: [$OEOMA_{500}$]/[initiator][EYH_2]/[$CuBr_2$]/[TPMA] = 600/1/0.03/x/x, [$OEOMA_{500}$] = 300 mM, [initiator] = 0.5 mM, [EYH_2] = 0.015 mM, [$CuBr_2$] = 0.3–1.2 mM, and [TPMA] = 0.9–3.6 mM in PBS at RT under green-LED irradiation for 30 min (λ = 520 nm, 3.7 mW cm^{-2}). GPC traces are shown in Figure S7. DNA initiator with an internal **SBiB** (T4-**SBiB**-T4) was used as a model DNA oligo initiator.

[a]Monomer conversion was determined by ^{1}H NMR spectroscopy.

[b]Number-average absolute molecular weight ($M_{n,abs}$) was determined by Mark-Houwink calibration according to the previously reported procedures.[60]

[c]Number-average apparent molecular weight ($M_{n,GPC}$) and dispersity ($Đ$) were determined by DMF GPC calibrated to polymethyl methacrylate (PMMA) standards.

[d]Reaction was conducted in 25% acetonitrile.

[e]Final concentration of NaCl was raised to 340 mM.

of the $[X–Cu/L]^{2+}$ deactivator[63–65] and protect the DNA phosphate backbone from electrostatic binding of the $[Cu^{II}/L]^{2+}$ complexes. Interestingly, the monomer conversion decreased from 80% to 67% (Table 1, entry 4), similar to the result with HEBiB (Table 1, entry 1), and a narrower molecular-weight distribution was obtained ($Đ$ = 1.27). This result implies that $[Cu^{II}/L]^{2+}$ complexes could interact with DNA predominantly through weak and reversible electrostatic interaction, and contamination of nucleic acids with copper through coordination is less preferred as a result of stable complexation of Cu with ATRP ligands (e.g., TPMA).[61] We also performed electrochemical analysis of Cu/TPMA binding to DNA by progressively adding salmon DNA to $CuBr_2$/TPMA complex in PBS (Figure S24). The negligible change in the cyclic voltammetry graph suggests that there is no evident binding of DNA to the catalyst. Further, a series of control experiments on polymerization in the presence of other DNA (Tables S4 and S5) showed that higher DNA concentrations in the reaction mixture could result in polymers with higher monomer conversion and dispersity values.

The control experiments prompted us to examine whether we could tune the dispersity of the DNA-polymer hybrids by simply altering the concentration of the Cu complex. As shown in entries 5–8 (Table 1), increasing the $CuBr_2$/TPMA concentration resulted in lower monomer conversion and dispersity.[63,66] Under the conditions tested, we achieved dispersity values in the range of 1.20–1.35. This indicates that the dispersity of polymer chains grown from DNA can be tuned, offering another route for tailoring the properties and functionality of DNA-polymer hybrids.[67,68] Of note, entry 7 in Table 1 was chosen as the standard polymerization conditions and used hereafter in this study because molar ratios of [$OEOMA_{500}$]/[T4-**SBiB**-T4] [EYH_2]/[$CuBr_2$]/[TPMA] = 600/1/0.03/1.8/5.4 provided acceptable monomer conversion (57%) and low dispersity ($Đ$ = 1.23) in 30 min, along with a reasonable deviation between the theoretical molecular weight ($M_{n,th}$), the number-average absolute molecular weight ($M_{n,abs}$), and the apparent molecular weight ($M_{n,GPC}$) (GPC = gel permeation chromatography).

Reliability of the SBiB reagent within an oligonucleotide sequence

The performance of the T4-**SBiB**-T4 macroinitiator in EY/Cu-catalyzed ATRP was investigated under optimized conditions (0.9 mM of $CuBr_2$ and 2.7 mM of TPMA; Figure 2). As

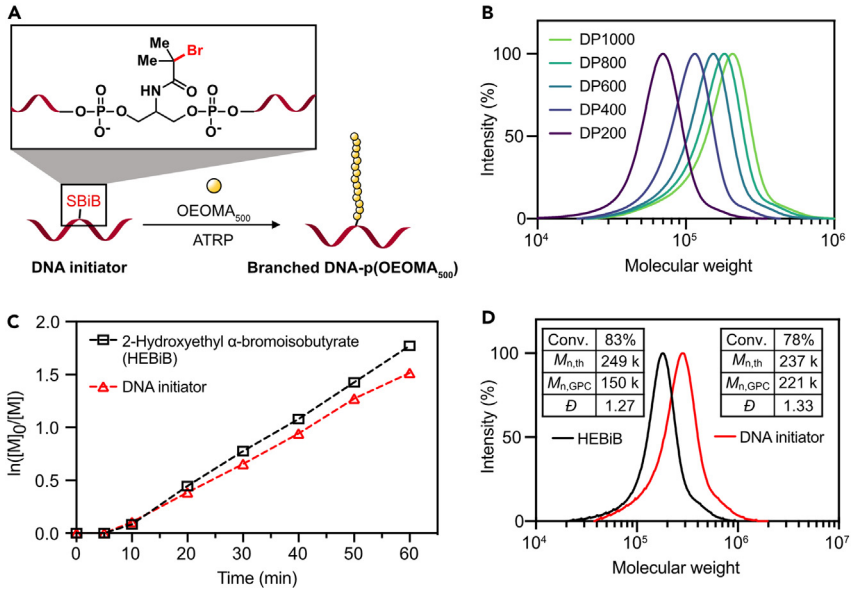

Figure 2. Controlled polymerization from the SBiB in the middle of DNA

All polymerizations were performed under the standard polymerization conditions ([$OEOMA_{500}$] = 300 mM, [EYH_2] = 0.015 mM, [$CuBr_2$] = 0.9 mM, [TPMA] = 2.7 mM) and analyzed by DMF GPC (calibrated to polymethyl methacrylate [PMMA]). T4-**SBiB**-T4 DNA initiator was used as a model initiator (see Table S3 for the sequence of the DNA initiator).

(A) Schematic illustration of grafting from **SBiB** located in the center of DNA; the inset shows the structure of the incorporated SBiB initiator residue.

(B) Molecular-weight control of the polymer chain grafted from the middle of DNA after 30 min of ATRP. The molecular weight was controlled by changes in the initiator concentration ([T4-**SBiB**-T4] = 0.3–1.5 mM). The monomers conversion and dispersity of the GPC traces are shown in Table S6.

(C) First-order kinetic plots of polymerizations using HEBiB (black line) and DNA initiator (red line).

(D) GPC traces of the polymer grafted from HEBiB (black line) and DNA (red line) after 60 min of reaction.

demonstrated in Figure 2B, the DNA initiator with **SBiB** in the middle showed good molecular-weight control, showed a monomodal GPC trace with low dispersity (Table S6), and followed a behavior of controlled polymerization similar to that of the HEBiB initiator (Figure 2C),[69] suggesting that there is a little steric constraint at the initiation site. The kinetic study revealed that after a short inhibition period of 5 min, the monomer conversion evolved linearly until it reached 78% after 60 min of green-light irradiation (Figures S10 and S11). The resulting DNA-polymer hybrid was further analyzed by GPC, which showed a reasonably narrow molecular-weight distribution of 1.33 (Figure 2D). However, the $M_{n,GPC}$ of DNA-polymer conjugates was higher than that of the control experiment acquired with conventional ATRP initiator (i.e., HEBiB). This was most likely due to the termination reaction, which is evident from the decreased monomer consumption between 50 and 60 min in Figure 2C.

We also investigated the steric hindrance to polymerization from an initiator incorporated in the middle of a DNA sequence. Three different DNA initiators with different degrees of crowding were prepared (DNA with internal **SBiB**, DNA with a terminal **SBiB**, and DNA with our previously reported terminal ATRP initiator, which has a four-carbon spacer)[45] as shown in Figure S12. Interestingly, polymerizations from all the DNA initiators showed compatible conversions (60%–64%) and low dispersity ($1.18 < Đ < 1.2$). These results demonstrate that the steric hindrance to grafting from the middle of DNA is negligible and that well-controlled polymerization

from **SBiB** within DNA can be expected, regardless of its position, despite the smaller inter-nucleotide distance (ca. 0.34 nm) than that of commonly used PEG-like monomers (e.g., $OEOMA_{500}$ and $OEOMA_{300}$).

DNA initiators still attached to the solid support could be useful for the polymerization of hydrophobic monomers beyond PEG-like monomers and the synthesis of nucleic-acid-polymer amphiphiles.[45] We therefore took advantage of the T8-**SBiB** model DNA initiator still on the controlled pore glass (CPG) solid support and used methyl acrylate (MA) as the model hydrophobic monomer for polymerization. Notably, we added ethyl α-bromoisobutyrate (EBiB) as the sacrificial initiator to increase the deactivator concentration $[X–Cu^{II}/L]^{2+}$ and suppress undesired terminations.[70] After polymerization in DMSO under green-light irradiation and subsequent washing following the cleavage process, the resulting DNA-poly(MA) block copolymer (DNA-pMA) was characterized by DMF GPC (Figure S13). The small deviation between the $M_{n,th}$ and $M_{n,GPC}$, as well as a low dispersity of 1.15, indicated the successful synthesis of DNA amphiphile by ATRP from the solid support.

Versatility of the SBiB reagent: Incorporating multiple initiators and using it with photocleavable linkers and in duplex DNA

Next, we investigated the applicability of our methodology to the preparation of more complex DNA-polymer hybrids by incorporating multiple **SBiB** initiators in different positions in DNA sequences. We prepared three different DNA-**SBiB** initiators with five **SBiB** moieties in different positions: one with five consecutive **SBiB** initiators, all at the 5′ terminus (T8-*t*-**SBiB5**); one with five consecutive **SBiB**s in the middle of a T8 sequence (T8-*m*-**SBiB5**); and five **SBiB**s spread within a T8 sequence such that there was one thymidine residue between the **SBiB** units (T8-*s*-**SBiB5**). After the polymerization from the DNA initiators, we purified the DNA-polymer hybrid by using a 100K molecular-weight cutoff (MWCO) filter and C18 cartridge and characterized it by size-exclusion chromatography equipped with a multi-angle light-scattering detector (SEC-MALS) by using PBS as an eluent. The results shown in Figures 3A–3C demonstrate that a well-defined polymer chain was grown from each of the DNA initiators. Notably, we observed only a small deviation between the $M_{n,th}$ and the number-average molecular weight obtained from SEC-MALS ($M_{n,MALS}$), as well as a low dispersity despite the presence of multiple initiators. This indicates that the method can be used to engineer more complex multi-grafted polymer architectures from initiators incorporated with single-nucleotide precision within sequences.

For the synthesis of multi-branched bioconjugates, simultaneous initiation is often a critical parameter that leads to well-defined concurrent polymer growth from all initiation sites.[71,72] To more carefully examine the homogeneity of polymers grafted from different **SBiB** initiators within a single DNA molecule, we designed a T12 DNA initiator with three **SBiB** residues containing photocleavable (pc) *o*-nitrobenzyl linkers between **SBiB** units (T12-*pc*-**SBiB3**; Figure 3D). Initially, photo-ATRP was performed with T12-*pc*-**SBiB3** as the initiator under optimized polymerization conditions with a target degree of polymerization (DP) of 800. We purified the resulting DNA-polymer hybrid with a 100K MWCO filter and C18 reverse-phase column to remove unreacted monomer and photocatalyst. The monomodal GPC trace and low dispersity of 1.11 indicated successful polymerization (Figure 3D, black line). After this analysis, we irradiated a vial containing the DNA-polymer hybrid with UV light (λ = 365 nm, 6.0 mW cm^{-2}) for 5 min to cleave the pc linker in the DNA backbone and release the polymer chains. These cleaved polymer chains were analyzed by SEC-MALS (Figure 3D, red line). The released polymers showed a monomodal

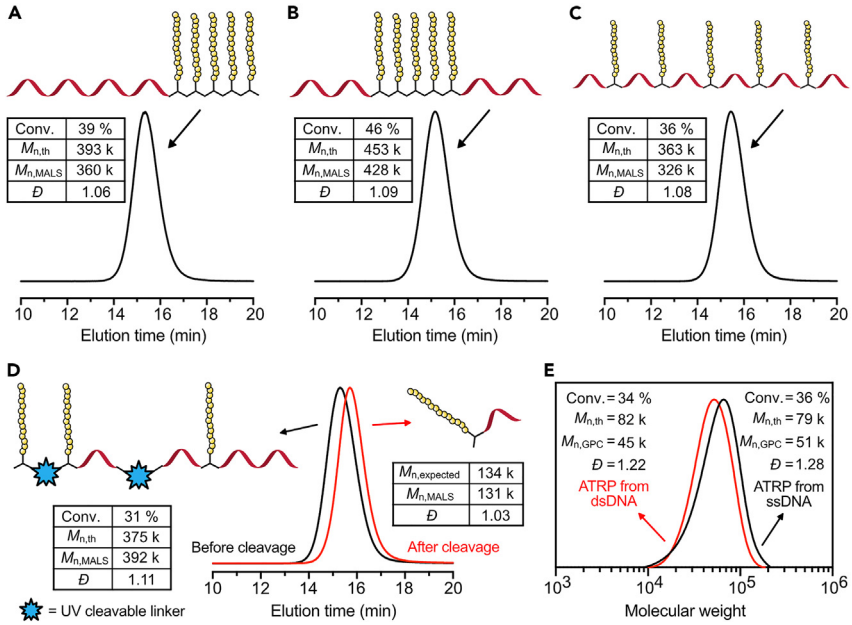

Figure 3. Grafting from DNA with multiple SBiB residue and topology control

(A–C) SEC-MALS traces of DNA with (A) five terminal polymer moieties, (B) five internal polymer moieties, and (C) five spread internal polymers. Standard polymerization conditions at the target DP of 400 were adopted: [DNA initiator] = 0.15 mM (i.e., 0.75 mM of **SBiB**). T8-*t*-**SBiB5**, T8-*m*-**SBiB5**, and T8-*s*-**SBiB5** were used as the initiator for (A), (B), and (C), respectively.

(D) SEC-MALS traces of DNA-polymer hybrids before and after UV cleavage. T12-*pc*-**SBiB3** DNA initiator, which contains UV-cleavable linkers between **SBiB** residue, was used. The polymerization was performed under the standard condition at the target DP of 800: [DNA initiator] = 0.125 mM (i.e., 0.375 mM of **SBiB**). UV light (λ = 365 nm, 6.0 mW cm^{-2}) was irradiated for 10 min to cleave polymer tethers from DNA.

(E) Aqueous GPC (calibrated to poly(acrylic acid) standards) traces of DNA-polymer grafted from 21-mer ssDNA initiator (Beta-**SBiB1**, black line) and dsDNA initiator (Beta-**SBiB1** forming a duplex with Beta*, red line) under the standard polymerization condition (target DP of 600).

and symmetrical curve with narrow molecular-weight distribution (*Đ* = 1.03). In addition, the $M_{n,MALS}$ (131,000) was nearly one-third of the molecular weight obtained before cleavage ($M_{n,th}$ = 134,000)—corresponding well with the three different initiators that were on the T12-*pc*-**SBiB3** sequence. We could thereby confirm the homogeneity of the multiple polymer chains simultaneously initiated and grafted from the **SBiB** residues integrated into the distinct locations interspersed within a single oligonucleotide molecule.

Hybridization-driven self-assembly has made DNA a versatile building material for nanoscience.[73] We envisioned that the sequence control over **SBiB** incorporation in DNA could expand the availability of DNA initiators as new precursors for the fabrication of hybrid nanomaterials. Toward this end, we first examined the hybridization of a mixed oligonucleotide sequence containing an internal **SBiB** initiator residue in the middle (Beta-**SBiB1**) with a stoichiometric amount of complementary DNA and then performed temperature annealing. For the hybridization experiments, we used two different strands complementary to Beta-**SBiB1**: one that was fully complementary to the Beta sequence (Beta*) and another that was fully complementary to the beta sequence with the additional inclusion of a mismatched T residue opposite the **SBiB** location within the beta sequence (Beta*$_{Tmm}$). We used Beta*$_{Tmm}$ to evaluate whether the single T residue opposite the **SBiB** could reduce the strain during duplex formation (Figure S14). Through native gel electrophoresis,

we observed that Beta-**SBiB1** could successfully hybridize with both Beta* and Beta*$_{Tmm}$ (Figure S14). Further, we found that even DNA with two internal **SBiB** moieties (Beta-**SBiB2**) could form a duplex without leaving unhybridized single-stranded DNA (ssDNA) (Figure S15).

To illustrate the potential of **SBiB**-modified DNA duplexes for nanofabrication, we attempted to graft from **SBiB** in the middle of annealed duplex DNA. Note that under the duplex DNA initiator, the strands underwent heating to 95°C for the annealing process. The general EY/Cu-catalyzed ATRP conditions in 1× PBS at room temperature (RT) were used with the DNA duplex initiator, and the polymer hybrid was analyzed by GPC. Interestingly, the polymerization from ssDNA (Beta-**SBiB1**) and double-stranded DNA (dsDNA) (Beta-**SBiB1** + Beta* duplex) showed comparable conversion and dispersity (Figure 3E). The conversions from both experiments were slightly lower than previous results with shorter oligoT initiator (T4-**SBiB**-T4; Table 1, entry 7), which could be attributed to the intrinsic nature of grafting from a macroinitiator. Interestingly, the polymer chains initiated from dsDNA (Figure 3E, red line) showed a slightly narrower molecular-weight distribution, which was most likely due to the bulged-out **SBiB** from the duplex[74] and the conformational rigidity (persistence length of 50 nm).[75]

Thermal stability of DNA structures modified with polymers

The thermal stability of the Beta-**SBiB1**/Beta* duplex was then investigated by melting curve analysis (Figure S16). The Beta-**SBiB1**/Beta* duplex was stained with EvaGreen dye, and the mixture was gradually heated from RT to 95°C while the fluorescence drop of EvaGreen was recorded via real-time PCR in 1× PBS. We observed a slightly lower melting temperature (T_m) for the DNA initiator duplex (68.4°C) and the DNA-pOEOMA duplex (65.2°C) than for the unmodified DNA duplex (73.5°C), which was similar to that of an abasic residue.[76] Next, we proceeded to measure the T_m of more complex DNA-polymer conjugates (Figure 4). For these analyses, a DNA strand containing five **SBiB** residues (Beta-**SBiB5**) was synthesized and utilized as the initiator yielding the ssDNA with five polymer tethers (Beta-p(OEOMA)5, $M_{n,MALS}$ = 484,000), as shown in Figure S17A. We then hybridized Beta-p(OEOMA)5 with its complementary DNA (Beta*) to form the Beta-p(OEOMA)5 duplex and utilized it for melting analysis. Of note, we additionally added 20 mM $MgCl_2$ to the buffer for melting curve analysis in order to enhance the stability of the duplex. We found that the thermal stability of the 21-bp DNA duplex was not significantly affected by the incorporation of five polymer chains and observed a T_m of 69.1°C, which was similar to that of the DNA initiator duplex (i.e., Beta-**SBiB5** duplex, T_m of 69.4°C), indicating that the polymer chains are not more disruptive to hybridization than the **SBiB** inserts in the backbone. This could be attributed to the stronger ionic strength than under the conditions in Figure S16, as well as the macromolecular excluded volume effect, which promotes hybridization.[20,77] We further explored whether modifications outside the duplex region affect hybridization. For this study, we synthesized DNA hairpins with an **SBiB** initiator positioned at one of two non-duplex locations: either in the middle of the loop (Alpha-*m*-**SBiB1**) or extended at the 5′ terminus (Alpha-*t*-**SBiB1**). As shown in Figure 4B, the three hairpin analogs exhibited nearly identical T_m values for the 12-bp stem. In addition, the data indicate that the polymerization from **SBiB** in the hairpin initiator did not significantly affect the stability of the duplex. Thus, the hybridization of nucleic acid initiators or their corresponding polymer hybrids can be engineered via strategic positioning of the modifications, in addition to ionic strength and sequence designs, including sequence length or GC content.

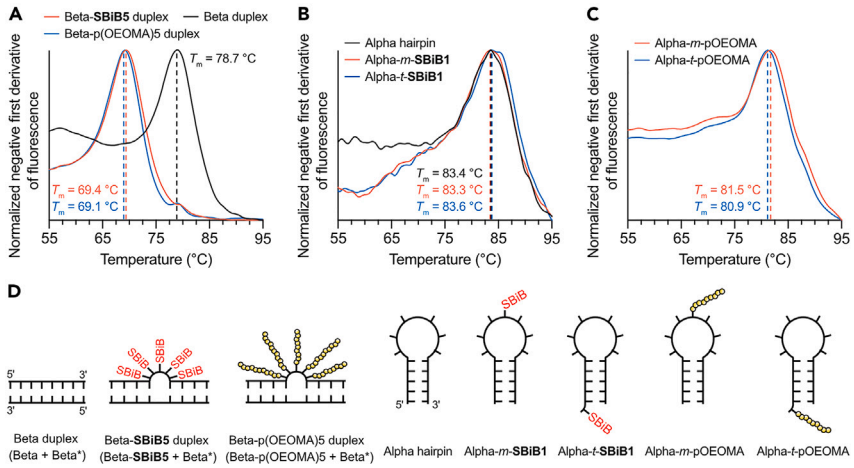

Figure 4. Thermal stability of DNA structures with initiators or polymers

SEC-MALS traces of the DNA-polymer hybrids are shown in Figure S17. Sequences of the DNA initiators are shown in Table S3.

(A) Melting curve analyses of the three types of DNA duplexes: the unmodified DNA duplex (Beta duplex), the DNA duplex with five initiators (Beta-**SBiB5** duplex), and the DNA duplex with five polymers (Beta-p(OEOMA)5 duplex).

(B) Melting curve analyses of the three types of DNA hairpins: the unmodified DNA hairpin (alpha hairpin), the DNA hairpin with one initiator in the middle of the loop (Alpha-*m*-**SBiB1**), and the DNA hairpin with one initiator on the 5′ terminus (Alpha-*t*-**SBiB1**).

(C) Melting curve analyses of the DNA hairpins with a polymer chain in the middle of the loop (Alpha-*m*-pOEOMA) or on the 5′ terminus (Alpha-*t*-pOEOMA).

(D) Schematics of DNA structures used for melting curve analysis.

Enhanced stability to nucleases

Although the sequence specificity, programmable self-assembly, and bioactivity of nucleic acids make them a critical and promising component of next-generation diagnostics, therapeutics, and biomaterials, the disadvantages of oligonucleotides alone, such as poor bioavailability, cellular uptake, and low nuclease resistance, significantly hinder their effectiveness. Chemically modified nucleotides or the incorporation of non-natural residues and linkages has been crucial in restricting the enzymatic degradation of nucleic acids.[78] Notably, the size, density, and location of the modified residue affect the stability of DNA.[20,79] Inspired by the previous findings, we investigated the polymer-assisted stabilization of DNA in 10% fetal bovine serum (FBS). Beta-**SBiB3** and Beta-**SBiB1** (middle only) were used as the initiator for polymerization under the optimized conditions, and the resulting Beta-p(OEOMA)3 was purified by a MWCO filter and polyacrylamide-gel electrophoresis (PAGE). SEC-MALS characterization showed a low dispersity of 1.10 and a molecular weight of 297,000, implying that the poly(OEOMA)$_{193}$ chains were attached on the 5′ and 3′ ends and in the middle of the beta sequence (Figure S18). To evaluate their resistance to degradation, we incubated unmodified beta DNA, Beta-**SBiB3** initiator, and OEOMA$_{500}$-grafted Beta-**SBiB** (Beta-p(OEOMA)3) at a final concentration of 5.3 μM in 10% FBS and 1× PBS at 37°C for 0–24 h and analyzed them by gel electrophoresis (Figure S19). As shown in Figure 5, unmodified beta DNA incubated in the presence (blue line) or absence (red line) of the free pOEOMA in the supernatant was entirely degraded within 12 h, whereas small-molecule-modified DNA (Beta-**SBiB3**, pink line) was 46% degraded after 24 h. Conversely, 89% of the Beta-p(OEOMA)3 (black line) survived after 24 h of incubation in 10% FBS, mainly because the bulky polymer tether effectively inhibited the binding of nucleases to DNA. The degradation of Beta-p(OEOMA)3 under the treatment of specific nucleases was also

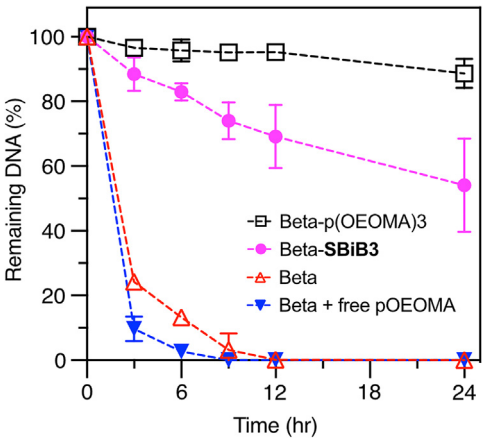

Figure 5. Degradation profile of modified and unmodified DNA in 10% FBS

Beta-p(OEOMA)3 was modified with three poly($OEOMA_{500}$)$_{194}$ tethers. The amount of remaining DNA was determined by measurement of the intensity of stained DNA after gel electrophoresis (Figure S19). Error bars represent standard deviations calculated from three different experiments. pOEOMA ($M_{n,MALS}$ = 169,000) initiated from HEBiB was used as the free polymer in the supernatant.

investigated (Figure S20). 52% and 7% of Beta-p(OEOMA)3 survived after the treatment of DNase I and exonuclease VII, respectively, indicating the possible degradation of polymer-modified DNA by both exo- and endonucleases.

Incorporation of SBiB and polymerizations from SBiB in RNA

Finally, we extended the **SBiB** incorporation methodology to RNA sequences. The solid-phase synthesis of RNA is similar to that of DNA with an important additional step for the final deprotection of the 2′-hydroxyl after cleavage from the solid support and deprotection of the nucleobase and phosphate protecting groups (Table S7). We began by examining **SBiB** stability under 2′-hydroxyl deprotection conditions by using triethylamine trihydrofluoride (TEA·3HF). We prepared and utilized model DNA initiators (T10-**SBiB**) with or without treatment of TEA·3HF (2.5 h at 65°C) to benchmark polymerization. The RNA-polymer hybrids were characterized by ^{1}H NMR and SEC-MALS. As shown in Figure S21, the compatible monomer conversion and the $M_{n,MALS}$ were observed regardless of the TEA·3HF treatment, demonstrating the stability of **SBiB** under 2′-hydroxyl deprotection conditions.

Having demonstrated the additional stability of **SBiB** under RNA deprotection conditions, we investigated the capability of the **SBiB** residue in RNA to initiate controlled polymerization. First, we synthesized a 20-mer model RNA with **SBiB** on the 5′ terminus (U20-**SBiB**) by using an oligonucleotide synthesizer (MALDI-TOF; Figure S22) and then used it for the EY/Cu-catalyzed ATRP of $OEOMA_{500}$ under optimized conditions for DNA hybrids. As shown in the kinetic study (Figure 6A), the linear increase in ln($[M]_0$/[M]) over time implies that the RNA carried out controlled polymerization to reach a high monomer conversion of 74% (Figure S23). After 60 min of polymerization in PBS under green light, the RNA-polymer hybrid was analyzed by SEC-MALS. A low dispersity of 1.04 evidenced the well-controlled polymerization from the RNA initiator. In addition, SEC-MALS traces in Figure 6C demonstrate that simply changing the RNA initiator concentration for polymerization can control the molecular weight of the grafted polymer with a narrow molecular-weight distribution ($1.02 < Đ < 1.04$).

We also investigated simultaneous initiation from RNA initiator by using a U12 RNA initiator with two **SBiB** residues and a pc linker between **SBiB** units (U12-*pc*-**SBiB2**; Figures 6D and 6E). Monomodal and symmetrical traces were observed before and after cleavage. In addition, the $M_{n,MALS}$ of the cleaved polymer (Figure 6E, red line) was nearly half the molecular weight of the RNA-polymer conjugate before

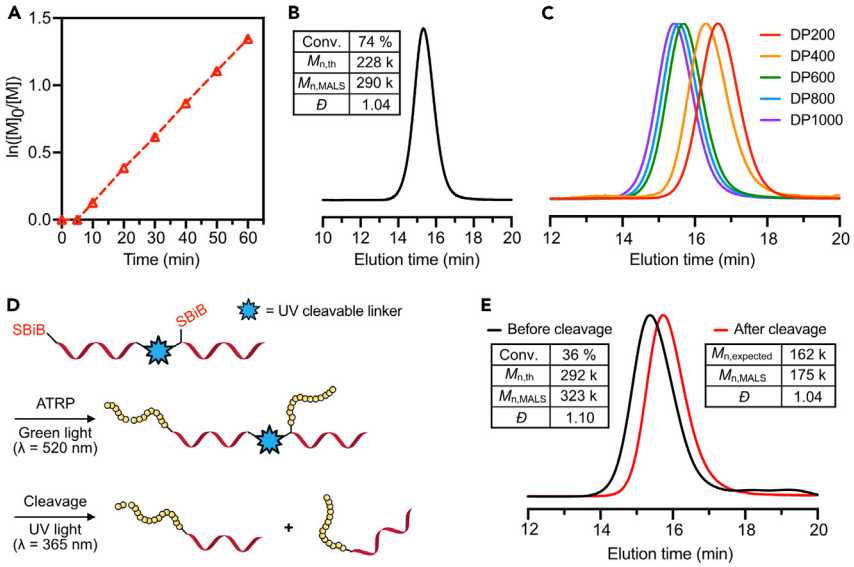

Figure 6. Controlled polymerization from RNA initiator

(A) Kinetic plots of the logarithm of $[M]_0/[M]$ over polymerization time. 20-mer uridine oligo with terminal **SBiB** (U20-**SBiB**) was used as a model initiator for the EY/Cu-catalyzed ATRP of $OEOMA_{500}$. Optimized polymerization conditions were employed: $[OEOMA_{500}]/[I]/[EYH_2]/[CuBr_2]/[TPMA]$ = 600/1/0.03/1.8/5.4 and $[OEOMA_{500}]$ = 300 mM in PBS under green-light irradiation for 60 min.

(B) SEC-MALS trace of RNA-poly($OEOMA_{500}$) after 60 min of photo-ATRP.

(C) Molecular-weight control of polymer chains grafted from RNA initiator. U20-**SBiB** was used as a model initiator for the EY/Cu-catalyzed ATRP of $OEOMA_{500}$. Standard polymerization condition was employed: $[OEOMA_{500}]/[I]/[EYH_2]/[CuBr_2]/[TPMA]$ = 600/0.3–1.5/0.03/1.8/5.4 and $[OEOMA_{500}]$ = 300 mM in PBS under green-light irradiation for 30 min. The monomer conversion and $Đ$ of each experiment are shown in Table S8.

(D and E) Investigation of simultaneous polymerizations from a single RNA strand. (D) Schematic illustration of grafting from polymerization and subsequent UV irradiation. (E) SEC-MALS traces of RNA-poly($OEOMA_{500}$) before and after UV irradiation. U12-*pc*-**SBiB2** RNA initiator, which contains UV-cleavable linkers between **SBiB** residue, was used. The polymerization was performed under the standard condition at the target DP of 800: [RNA initiator] = 0.188 mM (i.e., 0.375 mM of **SBiB**).

cleavage, indicating fast and concurrent initiation of polymerization from RNA. These results show that the use of the **SBiB**, even with RNA, remains a versatile and robust method that significantly expands access to possible NAPHs.[80]

Conclusions

In summary, we have developed the reagent and methodology for the precision fabrication of NAPHs, which were previously inaccessible. The **SBiB** phosphoramidite, a serinol-based ATRP-initiator-modified phosphoramidite, could be precisely located in any DNA or RNA sequence during solid-phase synthesis in single or multiple incorporations. EY/Cu-catalyzed ATRP using the **SBiB** initiator in the middle of an oligonucleotide sequence followed controlled radical behavior with good control over molecular weight and relatively low dispersity ($1.18 < Đ < 1.35$). Grafting from a sequence with multiple initiators and UV-induced cleavage of polymer chains confirmed the homogeneity of the polymer tethers grown from a DNA or RNA strand. The three-carbon linker of the **SBiB** initiator residue represents a minimal addition to an oligonucleotide phosphate backbone, similar to the three carbons of a natural residue between phosphates in the backbone of DNA or RNA. Duplex DNA in which the **SBiB** "residue" might be bulged out could be used for generating a duplex DNA-polymer hybrid. We also showed the enhanced remarkable degradation resistance of polymer-modified DNA (survival rate of 89%) in 10% FBS.

Together, these results suggest the potential application of **SBiB** in more complex, structured DNA-polymer architectures. We also demonstrated the first examples of a phosphoramidite approach to incorporating one or more initiators in RNA and subsequent RNA-polymer hybrids.

In combination with the developed **SBiB** phosphoramidite that can be used for incorporation in both DNA and RNA, our new oxygen-tolerant methods for ATRP use low copper and ligand concentrations that are more effective with DNA and RNA. Our method opens up tremendous opportunities for expanding the architectural scope of NAPHs in addition to the variety of methods for functionalizing polymers on a phosphate backbone by using a diverse library of phosphoramidite reagents—from fluorescent dyes and biofunctional molecules, such as biotin and cholesterol, to pc linkers that are available for solid-phase synthesis. We also anticipated that the ability to incorporate polymers anywhere in a folded functional DNA—as in quadruplexes, aptamers, and DNAzymes, as well as in the abundance of biofunctional folded RNA sequences—would provide unprecedented access to new NAPHs for a variety of biomedical applications, including drug delivery, biosensing, and microarray.

EXPERIMENTAL PROCEDURES

Full experimental procedures can be found in the supplemental information.

Resource availability

Lead contact

Requests for further information and resources should be directed to the lead contact, Krzysztof Matyjaszewski (km3b@andrew.cmu.edu).

Materials availability

All materials generated in this study are available from the lead contact.

Data and code availability

This study did not generate any code; all data generated during this study are available from the authors.

SUPPLEMENTAL INFORMATION

Supplemental information can be found online at https://doi.org/10.1016/j.chempr.2023.07.013.

ACKNOWLEDGMENTS

We gratefully acknowledge support from the National Science Foundation (DMR 2202747 to K.M.; MRI 2117784), Defense Threat Reduction Agency (HDTRA 1-20-1-0014 to J.J.), and the Polish National Agency for Academic Exchange (BPN/PPO/2022/1/00027 to G.S.). Dr. Francesca Lorandi is acknowledged for helping with the electrochemical analysis.

AUTHOR CONTRIBUTIONS

J.J., G.S., S.R.D., and K.M. conceived the project and wrote the manuscript. J.J. and G.S. conducted experiments. All authors edited the manuscript.

DECLARATION OF INTERESTS

A provisional patent application (no. 63/415712) on the invention, titled "Reagent that is equipped with polymerization initiation moiety on serinol scaffold for the

modification of synthetic oligonucleotide," was filed with the US Patent and Trademark Office.

INCLUSION AND DIVERSITY

We support inclusive, diverse, and equitable conduct of research.

Received: March 5, 2023
Revised: June 12, 2023
Accepted: July 21, 2023
Published: August 22, 2023

REFERENCES

1. Whitfield, C.J., Zhang, M., Winterwerber, P., Wu, Y., Ng, D.Y.W., and Weil, T. (2021). Functional DNA–polymer conjugates. Chem. Rev. *121*, 11030–11084.

2. Gačanin, J., Synatschke, C.V., and Weil, T. (2020). Biomedical applications of DNA-based hydrogels. Adv. Funct. Mater. *30*, 1906253.

3. Ishaqat, A., and Herrmann, A. (2021). Polymers strive for accuracy: from sequence-defined polymers to mRNA vaccines against COVID-19 and polymers in nucleic acid therapeutics. J. Am. Chem. Soc. *143*, 20529–20545.

4. Baker, S.L., Kaupbayeva, B., Lathwal, S., Das, S.R., Russell, A.J., and Matyjaszewski, K. (2019). Atom transfer radical polymerization for biorelated hybrid materials. Biomacromolecules *20*, 4272–4298.

5. Lückerath, T., Koynov, K., Loescher, S., Whitfield, C.J., Nuhn, L., Walther, A., Barner-Kowollik, C., Ng, D.Y.W., and Weil, T. (2020). DNA–polymer nanostructures by RAFT polymerization and polymerization-induced self-assembly. Angew. Chem. Int. Ed. Engl. *59*, 15474–15479.

6. Novak, S., Zhang, J., Kentzinger, E., Rücker, U., Portale, G., Jung, N., Jonas, U., Myung, J.S., Winkler, R.G., and Gompper, G. (2020). DNA self-assembly mediated by programmable soft-patchy interactions. ACS Nano *14*, 13524–13535.

7. Lu, X., Fu, H., Shih, K.C., Jia, F., Sun, Y., Wang, D., Wang, Y., Ekatan, S., Nieh, M.P., and Lin, Y. (2020). DNA-mediated step-growth polymerization of bottlebrush macromonomers. J. Am. Chem. Soc. *142*, 10297–10301.

8. Mondal, T., Nerantzaki, M., Flesch, K., Loth, C., Maaloum, M., Cong, Y., Sheiko, S.S., and Lutz, J.-F. (2021). Large sequence-defined supramolecules obtained by the DNA-guided assembly of biohybrid poly (phosphodiester)s. Macromolecules *54*, 3423–3429.

9. Trinh, T., Liao, C., Toader, V., Barłóg, M., Bazzi, H.S., Li, J., and Sleiman, H.F. (2018). DNA-imprinted polymer nanoparticles with monodispersity and prescribed DNA-strand patterns. Nat. Chem. *10*, 184–192.

10. Averick, S., Paredes, E., Li, W., Matyjaszewski, K., and Das, S.R. (2011). Direct DNA conjugation to star polymers for controlled reversible assemblies. Bioconjug. Chem. *22*, 2030–2037.

11. Li, Z., Zhang, Y., Fullhart, P., and Mirkin, C.A. (2004). Reversible and chemically programmable micelle assembly with DNA block-copolymer amphiphiles. Nano Lett. *4*, 1055–1058.

12. Rizzuto, F.J., Dore, M.D., Rafique, M.G., Luo, X., and Sleiman, H.F. (2022). DNA sequence and length dictate the assembly of nucleic acid block copolymers. J. Am. Chem. Soc. *144*, 12272–12279.

13. Zhang, C., Hernandez-Garcia, A., Jiang, K., Gong, Z., Guttula, D., Ng, S.Y., Malar, P.P., Van Kan, J.A., Dai, L., Doyle, P.S., et al. (2013). Amplified stretch of bottlebrush-coated DNA in nanofluidic channels. Nucleic Acids Res. *41*, e189.

14. Hernandez-Garcia, A., Werten, M.W., Stuart, M.C., de Wolf, F.A., and de Vries, R. (2012). Coating of single DNA molecules by genetically engineered protein diblock copolymers. Small *8*, 3491–3501.

15. Storm, I.M., Kornreich, M., Voets, I.K., Beck, R., de Vries, R., Cohen Stuart, M.A.C., and Leermakers, F.A. (2016). Loss of bottlebrush stiffness due to free polymers. Soft Matter *12*, 8004–8014.

16. Ruff, Y., Moyer, T., Newcomb, C.J., Demeler, B., and Stupp, S.I. (2013). Precision templating with DNA of a virus-like particle with peptide nanostructures. J. Am. Chem. Soc. *135*, 6211–6219.

17. Alemdaroglu, F.E., Zhuang, W., Zöphel, L., Wang, J., Berger, R.d., Rabe, J.P., and Herrmann, A. (2009). Generation of multiblock copolymers by PCR: synthesis, visualization and nanomechanical properties. Nano Lett. *9*, 3658–3662.

18. Fouz, M.F., Mukumoto, K., Averick, S., Molinar, O., McCartney, B.M., Matyjaszewski, K., Armitage, B.A., and Das, S.R. (2015). Bright fluorescent nanotags from bottlebrush polymers with DNA-tipped bristles. ACS Cent. Sci. *1*, 431–438.

19. Wang, Y., Wang, D., Jia, F., Miller, A., Tan, X., Chen, P., Zhang, L., Lu, H., Fang, Y., Kang, X., et al. (2020). Self-assembled DNA–PEG bottlebrushes enhance antisense activity and pharmacokinetics of oligonucleotides. ACS Appl. Mater. Interfaces *12*, 45830–45837.

20. Jia, F., Wang, D., Lu, X., Tan, X., Wang, Y., Lu, H., and Zhang, K. (2018). Improving the enzymatic stability and the pharmacokinetics of oligonucleotides via DNA-backboned bottlebrush polymers. Nano Lett. *18*, 7378–7382.

21. Tan, X., Lu, H., Sun, Y., Chen, X., Wang, D., Jia, F., and Zhang, K. (2019). Expanding the materials space of DNA via organic-phase ring-opening metathesis polymerization. Chem *5*, 1584–1596.

22. Rush, A.M., Thompson, M.P., Tatro, E.T., and Gianneschi, N.C. (2013). Nuclease-resistant DNA via high-density packing in polymeric micellar nanoparticle coronas. ACS Nano *7*, 1379–1387.

23. Yan, Y., Liu, L., Xiong, H., Miller, J.B., Zhou, K., Kos, P., Huffman, K.E., Elkassih, S., Norman, J.W., Carstens, R., et al. (2016). Functional polyesters enable selective siRNA delivery to lung cancer over matched normal cells. Proc. Natl. Acad. Sci. USA *113*, E5702–E5710.

24. Yu, Y., Guo, Y., Tian, Q., Lan, Y., Yeh, H., Zhang, M., Tasan, I., Jain, S., and Zhao, H. (2020). An efficient gene knock-in strategy using 5′-modified double-stranded DNA donors with short homology arms. Nat. Chem. Biol. *16*, 387–390.

25. Lu, X., Jia, F., Tan, X., Wang, D., Cao, X., Zheng, J., and Zhang, K. (2016). Effective antisense gene regulation via noncationic, polyethylene glycol brushes. J. Am. Chem. Soc. *138*, 9097–9100.

26. Li, H., Li, Y., Xiao, Y., Zhang, B., Cheng, Z., Shi, J., Xiong, J., Li, Z., and Zhang, K. (2020). Well-defined DNA–polymer miktoarm stars for enzyme-resistant nanoflares and carrier-free gene regulation. Bioconjug. Chem. *31*, 530–536.

27. Roloff, A., Nelles, D.A., Thompson, M.P., Yeo, G.W., and Gianneschi, N.C. (2018). Self-transfecting micellar RNA: modulating nanoparticle cell interactions via high density display of small molecule ligands on micelle coronas. Bioconjug. Chem. *29*, 126–135.

28. Averick, S.E., Paredes, E., Dey, S.K., Snyder, K.M., Tapinos, N., Matyjaszewski, K., and Das, S.R. (2013). Autotransfecting short interfering RNA through facile covalent polymer escorts. J. Am. Chem. Soc. *135*, 12508–12511.

29. Safak, M., Alemdaroglu, F.E., Li, Y., Ergen, E., and Herrmann, A. (2007). Polymerase chain reaction as an efficient tool for the preparation of block copolymers. Adv. Mater. *19*, 1499–1505.

30. Zhao, Z., Chen, C., Cao, T., Li, C., Shao, Y., Zhang, Y., Qiu, D., Shi, Q., and Fan, Q.H. (2018). Self-collapsing of single molecular poly-propylene oxide (PPO) in a 3D DNA network. Small *14*, 1703426.

31. Stiakakis, E., Jung, N., Adžić, N., Balandin, T., Kentzinger, E., Rücker, U., Biehl, R., Dhont, J.K.G., Jonas, U., and Likos, C.N. (2021). Self assembling cluster crystals from DNA based dendritic nanostructures. Nat. Commun. *12*, 7167.

32. Chen, C., Ng, D.Y.W., and Weil, T. (2020). Polymer bioconjugates: modern design concepts toward precision hybrid materials. Prog. Polym. Sci. *105*, 101241.

33. Liu, K., Zheng, L., Liu, Q., de Vries, J.W., Gerasimov, J.Y., and Herrmann, A. (2014). Nucleic acid chemistry in the organic phase: from functionalized oligonucleotides to DNA side chain polymers. J. Am. Chem. Soc. *136*, 14255–14262.

34. Wilks, T.R., Bath, J., de Vries, J.W., Raymond, J.E., Herrmann, A., Turberfield, A.J., and O'Reilly, R.K. (2013). "Giant surfactants" created by the fast and efficient functionalization of a DNA tetrahedron with a temperature-responsive polymer. ACS Nano *7*, 8561–8572.

35. Wilks, T.R., and O'Reilly, R.K. (2016). Efficient DNA–polymer coupling in organic solvents: a survey of amide coupling, thiol-ene and tetrazine–norbornene chemistries applied to conjugation of poly(N-isopropylacrylamide). Sci. Rep. *6*, 39192.

36. Sun, H., Yang, L., Thompson, M.P., Schara, S., Cao, W., Choi, W., Hu, Z., Zang, N., Tan, W., and Gianneschi, N.C. (2019). Recent advances in amphiphilic polymer–oligonucleotide nanomaterials via living/controlled polymerization technologies. Bioconjug. Chem. *30*, 1889–1904.

37. Zhang, C., Hao, L., Calabrese, C.M., Zhou, Y., Choi, C.H.J., Xing, H., and Mirkin, C.A. (2015). Biodegradable DNA-brush block copolymer spherical nucleic acids enable transfection agent-free intracellular gene regulation. Small *11*, 5360–5368.

38. Yang, L., Sun, H., Liu, Y., Hou, W., Yang, Y., Cai, R., Cui, C., Zhang, P., Pan, X., and Li, X. (2018). Self-assembled aptamer-grafted hyperbranched polymer nanocarrier for targeted and photoresponsive drug delivery. Angew. Chem. Int. Ed. *130*, 17294–17298.

39. Lu, X., Tran, T.H., Jia, F., Tan, X., Davis, S., Krishnan, S., Amiji, M.M., and Zhang, K. (2015). Providing oligonucleotides with steric selectivity by brush-polymer-assisted compaction. J. Am. Chem. Soc. *137*, 12466–12469.

40. Heredia, K.L., Nguyen, T.H., Chang, C.W., Bulmus, V., Davis, T.P., and Maynard, H.D. (2008). Reversible siRNA–polymer conjugates by RAFT polymerization. Chem. Commun. 3245–3247.

41. Enciso, A.E., Fu, L., Lathwal, S., Olszewski, M., Wang, Z., Das, S.R., Russell, A.J., and Matyjaszewski, K. (2018). Biocatalytic "oxygen-fueled" atom transfer radical polymerization. Angew. Chem. Int. Ed. *57*, 16157–16161.

42. Zhang, L., Baker, S.L., Murata, H., Harris, N., Ji, W., Amitai, G., Matyjaszewski, K., and Russell, A.J. (2020). Tuning butyrylcholinesterase inactivation and reactivation by polymer-based protein engineering. Adv. Sci. *7*, 1901904.

43. Niu, J., Lunn, D.J., Pusuluri, A., Yoo, J.I., O'Malley, M.A., Mitragotri, S., Soh, H.T., and Hawker, C.J. (2017). Engineering live cell surfaces with functional polymers via cytocompatible controlled radical polymerization. Nat. Chem. *9*, 537–545.

44. Tokura, Y., Jiang, Y., Welle, A., Stenzel, M.H., Krzemien, K.M., Michaelis, J., Berger, R., Barner-Kowollik, C., Wu, Y., and Weil, T. (2016). Bottom-up fabrication of nanopatterned polymers on DNA origami by in situ atom-transfer radical polymerization. Angew. Chem. Int. Ed. *128*, 5786–5791.

45. Averick, S.E., Dey, S.K., Grahacharya, D., Matyjaszewski, K., and Das, S.R. (2014). Solid-phase incorporation of an ATRP initiator for polymer-DNA biohybrids. Angew. Chem. Int. Ed. *53*, 2739–2744.

46. Broyer, R.M., Quaker, G.M., and Maynard, H.D. (2008). Designed amino acid ATRP initiators for the synthesis of biohybrid materials. J. Am. Chem. Soc. *130*, 1041–1047.

47. Lin, E.-W., and Maynard, H.D. (2015). Grafting from small interfering ribonucleic acid (siRNA) as an alternative synthesis route to siRNA–polymer conjugates. Macromolecules *48*, 5640–5647.

48. Lee, Y., Kwon, Y., Kim, Y., Yu, C., Feng, S., Park, J., Doh, J., Wannemacher, R., Koo, B., Gierschner, J., and Kwon, M.S. (2022). A water-soluble organic photocatalyst discovered for highly efficient additive-free visible-light-driven grafting of polymers from proteins at ambient and aqueous environments. Adv. Mater. *34*, e2108446.

49. Lathwal, S., Yerneni, S.S., Boye, S., Muza, U.L., Takahashi, S., Sugimoto, N., Lederer, A., Das, S.R., Campbell, P.G., and Matyjaszewski, K. (2021). Engineering exosome polymer hybrids by atom transfer radical polymerization. Proc. Natl. Acad. Sci. USA *118*. e2020241118.

50. Yerneni, S.S., Lathwal, S., Cuthbert, J., Kapil, K., Szczepaniak, G., Jeong, J., Das, S.R., Campbell, P.G., and Matyjaszewski, K. (2022). Controlled release of exosomes using atom transfer radical polymerization-based hydrogels. Biomacromolecules *23*, 1713–1722.

51. Layadi, A., Kessel, B., Yan, W., Romio, M., Spencer, N.D., Zenobi-Wong, M., Matyjaszewski, K., and Benetti, E.M. (2020). Oxygen tolerant and cytocompatible iron(0)-mediated ATRP enables the controlled growth of polymer brushes from mammalian cell cultures. J. Am. Chem. Soc. *142*, 3158–3164.

52. Kim, J.Y., Lee, B.S., Choi, J., Kim, B.J., Choi, J.Y., Kang, S.M., Yang, S.H., and Choi, I.S. (2016). Cytocompatible polymer grafting from individual living cells by atom-transfer radical polymerization. Angew. Chem. Int. Ed. *55*, 15306–15309.

53. Truong, N.P., Jones, G.R., Bradford, K.G.E., Konkolewicz, D., and Anastasaki, A. (2021). A comparison of RAFT and ATRP methods for controlled radical polymerization. Nat. Rev. Chem. *5*, 859–869.

54. Beaucage, S.L., and Caruthers, M.H. (1981). Deoxynucleoside phosphoramidites—a new class of key intermediates for deoxypolynucleotide synthesis. Tetrahedron Lett. *22*, 1859–1862.

55. Kosuri, S., and Church, G.M. (2014). Large-scale de novo DNA synthesis: technologies and applications. Nat. Methods *11*, 499–507.

56. Cavallo, G., Al Ouahabi, A., Oswald, L., Charles, L., and Lutz, J.F. (2016). Orthogonal synthesis of "easy-to-read" information-containing polymers using phosphoramidite and radical coupling steps. J. Am. Chem. Soc. *138*, 9417–9420.

57. Al Ouahabi, A., Charles, L., and Lutz, J.F. (2015). Synthesis of non-natural sequence-encoded polymers using phosphoramidite chemistry. J. Am. Chem. Soc. *137*, 5629–5635.

58. Voirin, E., Behr, J.P., and Kotera, M. (2007). Versatile synthesis of oligodeoxyribonucleotide–oligospermine conjugates. Nat. Protoc. *2*, 1360–1367.

59. Jahns, H., Roos, M., Imig, J., Baumann, F., Wang, Y., Gilmour, R., and Hall, J. (2015). Stereochemical bias introduced during RNA synthesis modulates the activity of phosphorothioate siRNAs. Nat. Commun. *6*, 6317.

60. Szczepaniak, G., Jeong, J., Kapil, K., Dadashi-Silab, S., Yerneni, S.S., Ratajczyk, P., Lathwal, S., Schild, D.J., Das, S.R., and Matyjaszewski, K. (2022). Open-air green-light-driven ATRP enabled by dual photoredox/copper catalysis. Chem. Sci. *13*, 11540–11550.

61. Fantin, M., Isse, A.A., Gennaro, A., and Matyjaszewski, K. (2015). Understanding the fundamentals of aqueous ATRP and defining conditions for better control. Macromolecules *48*, 6862–6875.

62. Ribelli, T.G., Lorandi, F., Fantin, M., and Matyjaszewski, K. (2019). Atom transfer radical polymerization: billion times more active catalysts and new initiation systems. Macromol. Rapid Commun. *40*, e1800616.

63. Jones, G.R., Whitfield, R., Anastasaki, A., and Haddleton, D.M. (2016). Aqueous copper (II) photoinduced polymerization of acrylates: low copper concentration and the importance of sodium halide salts. J. Am. Chem. Soc. *138*, 7346–7352.

64. Szczepaniak, G., Łagodzińska, M., Dadashi-Silab, S., Gorczyński, A., and Matyjaszewski, K. (2020). Fully oxygen-tolerant atom transfer radical polymerization triggered by sodium pyruvate. Chem. Sci. *11*, 8809–8816.

65. Pan, X., Malhotra, N., Simakova, A., Wang, Z., Konkolewicz, D., and Matyjaszewski, K. (2015). Photoinduced atom transfer radical polymerization with ppm-level Cu catalyst by visible light in aqueous media. J. Am. Chem. Soc. *137*, 15430–15433.

66. Ribelli, T.G., Konkolewicz, D., Bernhard, S., and Matyjaszewski, K. (2014). How are radicals (re) generated in photochemical ATRP? J. Am. Chem. Soc. *136*, 13303–13312.

67. Yin, R., Wang, Z., Bockstaller, M.R., and Matyjaszewski, K. (2021). Tuning dispersity of linear polymers and polymeric brushes grown

from nanoparticles by atom transfer radical polymerization. Polym. Chem. *12*, 6071–6082.

68. Antonopoulou, M.N., Whitfield, R., Truong, N.P., Wyers, D., Harrisson, S., Junkers, T., and Anastasaki, A. (2022). Concurrent control over sequence and dispersity in multiblock copolymers. Nat. Chem. *14*, 304–312.

69. Matyjaszewski, K., and Xia, J. (2001). Atom transfer radical polymerization. Chem. Rev. *101*, 2921–2990.

70. Matyjaszewski, K., Miller, P.J., Shukla, N., Immaraporn, B., Gelman, A., Luokala, B.B., Siclovan, T.M., Kickelbick, G., Vallant, T., Hoffmann, H., et al. (1999). Polymers at interfaces: using atom transfer radical polymerization in the controlled growth of homopolymers and block copolymers from silicon surfaces in the absence of untethered sacrificial initiator. Macromolecules *32*, 8716–8724.

71. Matyjaszewski, K. (2018). Advanced materials by atom transfer radical polymerization. Adv. Mater. *30*, e1706441.

72. Matyjaszewski, K., and Tsarevsky, N.V. (2009). Nanostructured functional materials prepared by atom transfer radical polymerization. Nat. Chem. *1*, 276–288.

73. Seeman, N.C., and Sleiman, H.F. (2017). DNA nanotechnology. Nat. Rev. Mater. *3*, 1–23.

74. Mortensen, K.I., Sung, J., Flyvbjerg, H., and Spudich, J.A. (2015). Optimized measurements of separations and angles between intra-molecular fluorescent markers. Nat. Commun. *6*, 8621.

75. Roth, E., Glick Azaria, A., Girshevitz, O., Bitler, A., and Garini, Y. (2018). Measuring the conformation and persistence length of single-stranded DNA using a DNA origami structure. Nano Lett. *18*, 6703–6709.

76. Liu, Z., Ding, S., Kropachev, K., Jia, L., Amin, S., Broyde, S., and Geacintov, N.E. (2015). Resistance to nucleotide excision repair of bulky guanine adducts opposite abasic sites in DNA duplexes and relationships between structure and function. PLoS One *10*, e0137124.

77. Jia, F., Lu, X., Tan, X., Wang, D., Cao, X., and Zhang, K. (2017). Effect of PEG architecture on the hybridization thermodynamics and protein accessibility of PEGylated oligonucleotides. Angew. Chem. Int. Ed. *129*, 1259–1263.

78. Kulkarni, J.A., Witzigmann, D., Thomson, S.B., Chen, S., Leavitt, B.R., Cullis, P.R., and van der Meel, R. (2021). The current landscape of nucleic acid therapeutics. Nat. Nanotechnol. *16*, 630–643.

79. Gu, R., Oweida, T., Yingling, Y.G., Chilkoti, A., and Zauscher, S. (2018). Enzymatic synthesis of nucleobase-modified single-stranded DNA offers tunable resistance to nuclease degradation. Biomacromolecules *19*, 3525–3535.

80. Jeong, J., Hu, X., Murata, H., Szczepaniak, G., Rachwalak, M., Kietrys, A., Das, S.R., and Matyjaszewski, K. (2023). RNA-polymer hybrids via direct and site-selective acylation with the ATRP initiator and photoinduced polymerization. J. Am. Chem. Soc. *145*, 14435–14445.